Defect Structure and Electrical Conductivity of the Ruddlesden−Popper Phases $Sr_3FeMO_{6+\delta}$ (M = Co, Ni)

L. Mogni, F. Prado, and A. Caneiro*

Centro Atómico Bariloche, CNEA, 8400 S. C. de Bariloche RN, Argentina

Received February 17, 2006. Revised Manuscript Received May 18, 2006

In this work, we report a systematic study of the oxygen nonstoichiometry, high-temperature thermodynamics, and transport properties of the perovskite-related mixed conductor $Sr_3FeMO_{6+\delta}$ (M = Co, Ni). Thermogravimetry was used to determine the oxygen content change ($6+\delta$) as a function of temperature (T) and equilibrium oxygen partial pressure (pO_2) within the range 1×10^{-5} atm $< pO_2 <$ 1 atm and 400 °C $\leq T \leq$ 1000 °C. From the experimental values of the oxygen chemical potential (μ_{O_2}), we determined both the partial molar enthalpy (h_{O_2}) and the partial molar entropy (s_{O_2}) for the composition range $5.9 < 6+\delta < 6.6$. Thermodynamic data were fitted using a straightforward defect model. The model was deduced from the mass action law assuming oxygen-vacancy formation and involving different fractions of localized and delocalized charge carriers in iron sites and the metal transition M3d−O2p band, respectively. Electrical resistivity measurements as a function of pO_2 at constant temperature were performed in the 650 °C $\leq T \leq$ 1000 °C temperature range for $Sr_3FeCoO_{6+\delta}$ and $Sr_3FeNiO_{6+\delta}$ compounds. The activation energy values for the electrical-transport process at constant oxygen content values were obtained from the combination of electrical conductivity and thermogravimetry data. The electrical conductivity data are discussed within the frame of large polaron behavior in agreement with the thermodynamic data.

1. Introduction

Mixed-conductor oxides exhibiting both oxide-ion and electronic conduction are widely investigated because of their potential utilization in electrochemical applications, such as electrodes in SOFC, oxygen separation membranes, and methane conversion reactors.[1,2]

Early oxygen permeation and ionic conductivity studies[3−5] have shown that the perovskite phases $La_{1-x}Sr_xFe_{1-y}Co_yO_{3-\delta}$ exhibit high oxide-ion (0.01−1 S cm^{-1}) and electronic (1×10^2 to 1×10^3 S cm^{-1}) conductivities. The ionic conductivity in solid solution $La_{1-x}Sr_xFe_{1-y}Co_yO_{3-\delta}$ increases with the Sr and Co content because of the increment on the oxygen vacancy concentration, which improves the oxide-ion mobility in the lattice. However, large concentrations of oxygen vacancies may induce structural transformations to ordered structures as a consequence of the electrostatic interactions among oxygen defects.[6,7]

The search for new mixed-conductor oxides with a higher structural stability than the perovskite phases leads to the exploration of the mixed-conductor properties of the Ruddlesden−Popper series having the general formula $Sr_{n+1}Fe_nO_{3n+1}$. Phase crystal structure consists of n perovskite layers $SrFeO_3$ alternated with SrO rock-salt layers.[8] The $n = 2$ member of the series, $Sr_3Fe_2O_{6+\delta}$, has a crystal structure with tetragonal symmetry (space group *I*4/*mmm*) and tolerates a large oxygen nonstoichiometry that reaches a value of $\delta = 0$ at $T = 1000$ °C and $pO_2 = 1 \times 10^{-5}$ atm[9] without structural transformation. The substitution of Fe by Co increases the electrical conductivity, extends the range of oxygen nonstoichiometry ($5.5 \leq 6+\delta \leq 7$),[10] and improves the oxygen permeation fluxes across dense membranes, which is related to oxide-ion conductivity.[11−13] Recently, we have reported the synthesis and physical properties of novel compounds $Sr_3Fe_{2-x}Ni_xO_7$.[14,15] The partial substitution of Ni for Fe improves the electrical conductivity at low temperature.[14] At high temperatures, it extends the range of oxygen nonstoichiometry ($5.5 \leq 6+\delta \leq 7$) and increases the oxygen permeability without structural transformations[12,15] in a similar way as that of samples with Co.

* Corresponding author. E-mail: caneiro@cab.gov.ar. Fax: 54 2944 445299.

(1) Skinner, S. J. *Int. J. Inorg. Mater.* 2001 *3*, 113.
(2) Bouwmeester, H. J.; Burggraf, A. J. In *The CRC Handbook of Solid State Electrochemistry*; Gellings, P. J., Bouwmeester, H. J., Eds.; CRC Press: Boca Raton, FL, 1997; Chapter 14.
(3) Teraoka, Y.; Zhang, H. M.; Furukawa, S.; Yamazoe, N. *Chem. Lett.* **1985**, 1743.
(4) Teraoka, Y.; Nobunaga, T.; Yamazoe, N. *Chem. Lett.* **1988**, 503.
(5) Teraoka, Y.; Zhang, H. M.; Okamoto, K.; Yamazoe, N. *Mater. Res. Bull.* **1988**, *23*, 51.
(6) Prado, F.; Grunbaum, N.; Caneiro, A.; Manthiram, A. *Solid State Ionics* **2004**, *167*, 147.
(7) Grunbaum, N.; Mogni, L.; Prado, F.; Caneiro, A. *J. Solid State Chem.* **2004**, *177*, 2350.
(8) Ruddlesden, S. N.; Popper, P. *Acta Crystallogr.* **1958**, *11*, 54.
(9) Dann, S. E.; Weller, M. T.; Curie, D. B. *J. Solid State Chem.* **1992**, *97*, 179.
(10) Bréard, Y.; Michel, C.; Hervieu, M.; Studer, F.; Maignan, A.; Raveau, B. B. *Chem. Mater.* **2002**, *14*, 3128−3135.
(11) Armstrong, T.; Prado, F.; Manthiram, A. *Solid State Ionics* **2001**, *140*, 89.
(12) Prado, F.; Armstrong, T.; Caneiro, A.; Manthiram, A. *J. Electrochem. Soc.* **2001**, *148*, J7.
(13) Manthiram, A.; Prado, F.; Armstrong, T. *Solid State Ionics* **2002**, *152−153*, 647.
(14) Mogni, L.; Prado, F.; Ascolani, H.; Abbate, M.; Moreno, M. S.; Manthiram, A.; Caneiro, A. *J. Solid State Chem.* **2005**, *178*, 1559.
(15) Mogni, L.; Prado, F.; Caneiro, A.; Manthiram, A. *Solid State Ionics*, in press.

10.1021/cm0604007 CCC: $33.50
Published on Web 08/01/2006

Thermogravimetric and electrical-transport measurements of the equilibrium pO_2 as a function of temperature provide essential data on the thermodynamic stability, defect structure, and ionic- and electrical-transport mechanisms at the working temperature of the electrochemical applications. Although several studies were performed on the perovskite phases with La and Sr in the A site and Fe and Co in the B site,[6,7,16−24] this type of information is scarce for the Ruddlesden−Popper phases. Shilova et al.[25] reported the high-temperature thermodynamic and transport properties for solid solution $Sr_3(Fe,Ti)_2O_{6+\delta}$. Recently, we proposed a straightforward defect model assuming oxygen vacancies and localized charge carriers to explain the transport properties and reproduce the thermodynamic data of parent compound $Sr_3Fe_2O_{6+\delta}$.[26]

In this work, we study the effects of the substitution of Fe by Co or Ni in $Sr_3Fe_2O_{6+\delta}$ on the thermodynamic and electrical properties at high temperature. The dependence of the partial molar properties s_{O_2} and h_{O_2} on the oxygen content is discussed in terms of a defect model involving localized electronic states and delocalized electronic states within the frame of a rigid band model (RBM).[18,19] In addition, the electrical conductivity data are discussed in terms of the proposed defect model and the polaron theory.

2. Experimental Section

The $Sr_3FeCoO_{6+\delta}$ and $Sr_3FeNiO_{6+\delta}$ samples were synthesized by an acetic-based gel route using Fe, Ni, and Co acetates and $SrCO_3$ as raw materials.[12] The obtained gel was dried and decomposed at 450 °C for 30 min in air. An intermediate heat treatment was performed at 950 °C for 12 h in air. Dense samples were obtained by pressing the powders into pellets with a final heat treatment at 1300 °C under pure O_2 for 20 h. The cooling rate to room temperature was 1 °C/min. The presence of single-phase materials with the *I*4/*mmm* space group was checked by powder XRD. The homogeneity of the samples was confirmed by SEM observations and EDS analysis.

Isothermal measurements of the equilibrium pO_2 vs oxygen content $6+\delta$ were performed using highly sensitive thermogravimetric equipment[27] consisting of a symmetrical thermobalance based on a Cahn 1000 electrobalance coupled to an electrochemical gas blending system. This electrochemical system (zirconia pump and oxygen sensor)[28] provides a controlled $Ar-O_2$ atmosphere for the thermobalance, with pO_2 values ranging from 1×10^{-6} to 1 atm. The thermobalance allows for the determination of sample mass changes within ± 10 μg, i.e., for our samples of about 0.6 g of $Sr_3Fe_2O_{6+\delta}$, changes in $6+\delta$ were determined within ± 0.0003. The equilibrium criterion for the thermodynamic measurements was "constant sample weight with time, within ± 10 μg". This equilibrium criterion was verified over a period of 24 h for the low T and pO_2 range of measurements. The oxygen content was determined by in situ reduction in dry H_2 at 1000 °C assuming SrO, Fe, and Co or Ni as final products. The equilibrium pO_2 isotherms were measured within the T and pO_2 ranges 400 °C $\leq T \leq$ 1000 °C; 1×10^{-5} atm $\leq pO_2 \leq$ 1 atm.

DC resistivity measurements at high temperatures and controlled pO_2 were carried out by a standard four-probe method on a rectangular sample with dimensions 1.5 mm × 5 mm × 20 mm.

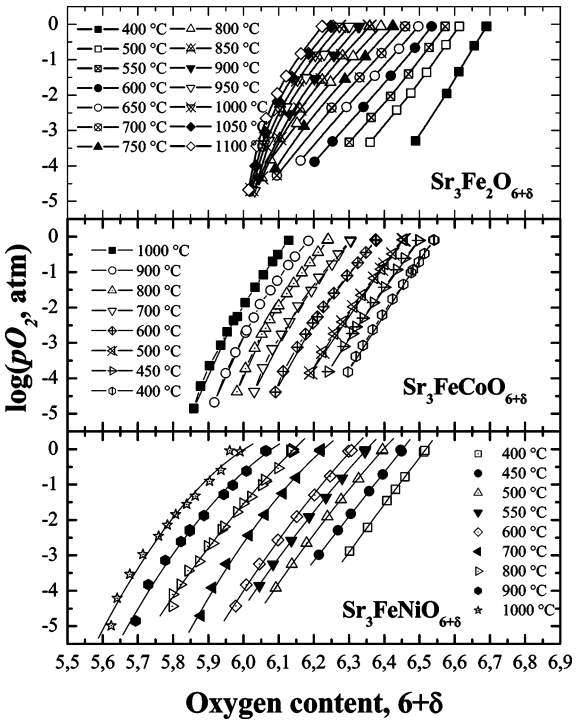

Figure 1. Isotherms of log pO_2 vs $6+\delta$ for $Sr_3Fe_2O_{6+\delta}$, $Sr_3FeCoO_{6+\delta}$, and $Sr_3FeNiO_{6+\delta}$ at several temperatures.

3. Results and Discussion

3.1. Thermodynamic Measurements and Partial Molar Properties. The equilibrium pO_2 isotherms as a function of oxygen content $6+\delta$ for $Sr_3FeCoO_{6+\delta}$ and $Sr_3FeNiO_{6+\delta}$ are displayed in Figure 1. In the same plot, we include for comparison the data for the $Sr_3Fe_2O_{6+\delta}$ compound taken from ref 26.

The pO_2 isotherms were reproduced by either increasing or decreasing pO_2. This fact indicates that the pO_2 values are representative of thermodynamic equilibrium states of the $Sr_3FeMO_{6+\delta}$ (M = Fe, Co, Ni) materials.

The $Sr_3FeCoO_{6+\delta}$ and $Sr_3FeNiO_{6+\delta}$ compounds do not show any phase transition within the T and pO_2 range of measurements in a manner similar to that found for $Sr_3Fe_2O_{6+\delta}$.[26]

(16) Patrakeev, M. V.; Leonidov, I. A.; Kozhevnikov, V. L.; Kharton, V. V. *Solid State Sci.* **2004**, *6*, 907.
(17) Lankhorst, M. H. R.; Ten Elshof, J. E. *J. Solid State Chem.* **1997**, *130*, 302.
(18) Lankhorst, M. H. R.; Bouwmeester, H. J. M.; Verweij, H. *Phys. Rev. Lett.* **1996**, *77*, 2989.
(19) Lankhorst, M. H. R.; Bouwmeester, H. J. M.; Verweij, H. *J. Solid State Chem.* **1997**, *133*, 555.
(20) Mizusaki, J.; Mima, Y.; Yamauchi, S.; Fueki, K. *J. Solid State Chem.* **1989**, *80*, 102.
(21) Mizusaki, J.; Yoshihiro, M.; Yamauchi, S.; Fueki, K. *J. Solid State Chem.* **1985**, *58*, 257.
(22) Sitte, W.; Bucher, E.; Preis, W. *Solid State Ionics* **2002**, *154−155*, 517.
(23) Bucher, E.; Sitte, W. *Solid State Ionics* **2004**, *173*, 23.
(24) Mitberg, R. B.; Patrakeev, M. V.; Leonidov, I. A.; Kozhevnikov, V. L.; Poeppelmeier, K. R. *Solid State Ionics* **2000**, *130*, 325.
(25) Shilova, Y. A.; Patrakev, M. V.; Mitberg, E. B.; Leonidov, I. A.; Kozhevnikov, V. L.; Poeppelmeier, K. R. *J. Solid State Chem.* **2002**, *168*, 275.
(26) Mogni, L.; Fouletier, J.; Prado, F.; Caneiro, A. *J. Solid State Chem.* **2005**, *178*, 2715.
(27) Caneiro, A.; Bavdaz, P.; Fouletier, J.; Abriata, J. P. *Rev. Sci. Instrum.* **1982**, *53*, 1072.
(28) Caneiro, A.; Bonnat, M.; Fouletier, J. *J. Appl. Electrochem.* **1981**, *11*, 83.

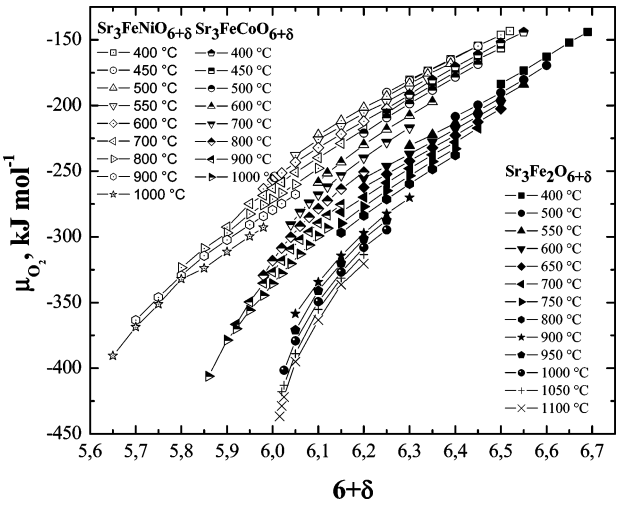

Figure 2. Oxygen chemical potential for $Sr_3Fe_2O_{6+\delta}$, $Sr_3FeCoO_{6+\delta}$, and $Sr_3FeNiO_{6+\delta}$ at several temperatures, obtained from the thermogravimetry data.

Although the isotherms for the $Sr_3Fe_2O_{6+\delta}$ material suggest the stabilization of the $Sr_3Fe_2O_6$ stoichiometric compound at high temperatures and low pO_2 values, those corresponding to $Sr_3FeCoO_{6+\delta}$ and $Sr_3FeNiO_{6+\delta}$ do not indicate the stabilization of compounds with oxygen content $6+\delta \approx 6.00$. The lower oxygen content values reached for compounds with Ni and Co with respect to that of pure Fe are related to a higher stabilization of mixed-valences states Co2+/Co3+ and Ni2+/Ni3+ with respect to those of Fe2+/Fe3+.

The replacement of Fe by Ni or Co in $Sr_3Fe_2O_{6+\delta}$ increases the oxygen nonstoichiometry range according to the series Fe < Co < Ni.

Form the equilibrium pO_2 values, the oxygen chemical potential μ_{O_2} can be computed by the following expression

$$\mu_{O_2}^{oxide}(P,T) = \mu_{O_2}^{gas}(P,T) = \mu_{O_2}^{0}(T) + RT\ln(pO_2) \qquad (1)$$

where $\mu_{O_2}^{0}(T)$ is the reference state at 1 atm (see ref 29), R the gas constant, and T the temperature in K.

The μ_{O_2}data vs $6+\delta$ for $Sr_3Fe_2O_{6+\delta}$, $Sr_3FeNiO_{6+\delta}$, and $Sr_3FeCoO_{6+\delta}$ are plotted in Figure 2. μ_{O_2} increases according to the series Fe < Co < Ni.

The shape of μ_{O_2} around $6+\delta = 6.00$ for the $Sr_3Fe_2O_{6+\delta}$ sample is quite different from those of $Sr_3FeNiO_{6+\delta}$ and $Sr_3FeCoO_{6+\delta}$. The rapid variation of the μ_{O_2} curvature for the $Sr_3Fe_2O_{6+\delta}$ as $6+\delta$ approaches 6.00 suggests an appreciable contribution of configurational entropy of the localized charge carriers in the Fe crystallographic sites (s_{conf}^{Fe}) to μ_{O_2} due to the stabilization of $Sr_3Fe_2O_6$ with all Fe as Fe3+.[26] On the contrary, the monotonic variation of μ_{O_2} around $6+\delta \approx 6.00$ for $Sr_3FeNiO_{6+\delta}$ and $Sr_3FeCoO_{6+\delta}$ materials would indicate a minor contribution of s_{conf}^{Fe}. This may be due to the presence of Fe4+, even for $6+\delta < 6.00$. Similar arguments about the contribution of s_{conf}^{Fe} to μ_{O_2} can be used to understand the smooth dependence of μ_{O_2} around $6+\delta \approx 6.50$ for the $Sr_3FeNiO_{6+\delta}$ and $Sr_3FeCoO_{6+\delta}$ compounds. This behavior of μ_{O_2}would suggest the existence of

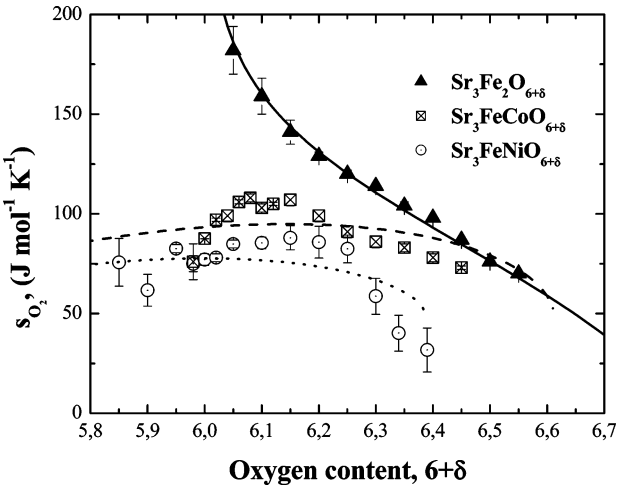

Figure 3. Partial molar entropy, s_{O_2}, as a function of the oxygen content $6+\delta$ for $Sr_3Fe_2O_{6+\delta}$, $Sr_3FeCoO_{6+\delta}$, and $Sr_3FeNiO_{6+\delta}$ compounds.

Fe3+ for $6+\delta > 6.5$. Even though the preferential oxidation of Fe3+ to Fe4+ should be expected, in agreement with literature data for Fe−Co perovskites,[30−31] the assumption of Fe3+ necessarily implies the simultaneous presence of Ni3+/Ni4+ or Co3+/Co4+ together with the Fe3+/Fe4+ for $6+\delta > 6.50$. The variation in defect concentration as a function of the oxygen content is discussed in the next section.

The partial molar properties s_{O_2} and h_{O_2} are related to μ_{O_2} through the equation

$$\mu_{O_2} = h_{O_2} - s_{O_2}T \qquad (2)$$

and can be computed by the following expressions

$$h_{O_2} = \left.\frac{\partial\left(\frac{\mu_{O_2}}{T}\right)}{\partial\left(\frac{1}{T}\right)}\right|_{\delta} \qquad (3)$$

$$s_{O_2} = -\left.\frac{\partial(\mu_{O_2})}{\partial(T)}\right|_{\delta} \qquad (4)$$

The s_{O_2} and h_{O_2} data for $Sr_3FeNiO_{6+\delta}$ and $Sr_3FeCoO_{6+\delta}$ are shown in Figures 3 and 4. We also include the values for $Sr_3Fe_2O_{6+\delta}$ taken from ref 26.

The behavior of both s_{O_2} and h_{O_2} as a function of $6+\delta$ is substantially different from that of $Sr_3Fe_2O_{6+\delta}$ reported in ref 26. For $Sr_3Fe_2O_{6+\delta}$, h_{O_2} increases slowly with $6+\delta$, and this behavior is associated with defect point interactions. h_{O_2} vs $6+\delta$ for $Sr_3FeNiO_{6+\delta}$ and $Sr_3FeCoO_{6+\delta}$ decreases rapidly as $6+\delta$ decreases. A similar behavior was reported for $(La,Sr)(Fe,Co)O_{3+\delta}$ perovskites and is associated with the contribution to h_{O_2} by the delocalized charge carriers created in the Co band.[17−21] In a similar way, we also assume for $Sr_3FeNiO_{6+\delta}$ and $Sr_3FeCoO_{6+\delta}$ compounds that the variations in h_{O_2} with $6+\delta$ are mainly related to the contribution of delocalized charge carriers in the Ni and Co bands.

(29) IUPAC Commission on Thermodynamics. *Oxygen: International Thermodynamics Tables of the Fluid State*; Blackwell Science: Oxford, U.K., 1987; Vol. 9.

(30) Evenrud, H.; Stølen, S. *J. Therm. Anal. Calorim.* **2002**, *69*, 795.

(31) Bakken, E.; Norby, T.; Stølen, S. *Phys. Chem. Chem. Phys.* **2006**, *8*, 429.

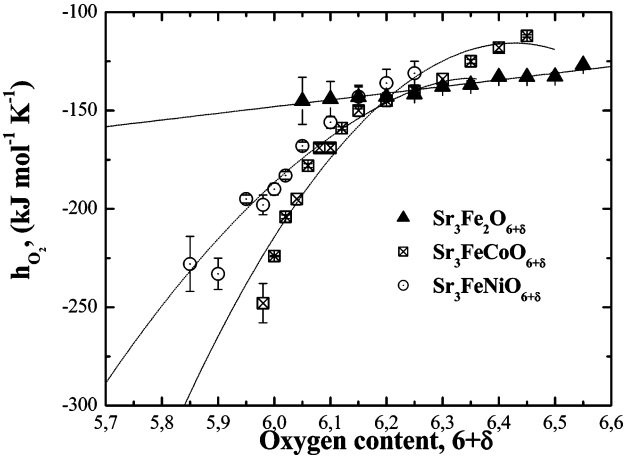

Figure 4. Partial molar enthalpy, h_{O_2}, as a function of $6+\delta$ for $Sr_3Fe_2O_{6+\delta}$, $Sr_3FeCoO_{6+\delta}$, and $Sr_3FeNiO_{6+\delta}$ compounds.

The variation in s_{O_2} with $6+\delta$ for $Sr_3FeNiO_{6+\delta}$ and $Sr_3FeCoO_{6+\delta}$ is also quite different from that of $Sr_3Fe_2O_{6+\delta}$. The $Sr_3Fe_2O_{6+\delta}$ compound exhibits localized charge carriers and the increment of s_{O_2} as $6+\delta$ approaches 6.00 is related to the formation of a compound with all Fe as Fe3+. The replacement of Fe by Ni and Co in $Sr_3Fe_2O_{6+\delta}$ prevents the formation of a compound with all Fe as Fe3+ at $6+\delta = 6.00$; this fact is evidenced in the behavior of s_{O_2} vs $6+\delta$ for both compounds.

3.2. Defect Model. In ref 26, we proposed a defect model for the oxygen incorporation in $Sr_3Fe_2O_{6+\delta}$ considering only localized charge carriers in the Fe site. It is worth mentioning that the presence of localized charge carriers is a common feature of the (La,Sr)$FeO_{3-\delta}$ perovskites.[16,20,21]

The defect equation using the Kröger−Vink notation for charge distributed in localized electronic states and double-charged oxygen vacancies is expressed by

$$2V_O^{\bullet\bullet} + O_2 + 4Fe_{Fe}^x \leftrightarrow 2O_O^x + 4Fe_{Fe}^{\bullet} \quad (5)$$

where $V_O^{\bullet\bullet}$ represents double-charged oxygen vacancies, O_O^x is a regular oxygen site, and $Fe_{Fe}^x/Fe_{Fe}^{\bullet}$ denotes an Fe3+/Fe4+ in the Fe crystallographic sites.

A different situation corresponds to the presence of delocalized charge carriers distributed in a partially filled transition metal M3d−O2p band. This is the case for (La,Sr)$CoO_{3-\delta}$ perovskites.[17−19]

The defect model equation for itinerant charge carriers is

$$2V_O^{\bullet\bullet} + O_2 + 2e' \leftrightarrow 2O_O^x \quad (6)$$

where e′ indicates an itinerant electron in the Co3d−O2p conduction band.

The simultaneous presence of Fe and Co in the B site of (La,Sr) perovskites would correspond to a situation intermediate to those described by eq 5 and eq 6.

In particular, for $La_{0.6}Sr_{0.4}Co_{1-y}Fe_yO_{3-\delta}$ compounds, Lankhorst et al.[17] proposed a defect model considering both eqs 5 and 6. A fraction f_e of the electrons involved in the defect reaction is taken from the Co3d−O2p conduction band, whereas the remaining fraction $1 - f_e$ electrons is distributed in the localized states of the iron sites.

The defect model reaction for this case can then be written as

$$2V_O^{\bullet\bullet} + O_2 + 4(1 - f_e)Fe_{Fe}^x + 4f_e e' \leftrightarrow 2O_O^x + 4(1 - f_e)Fe_{Fe}^{\bullet} \quad (7)$$

The exchange reaction of charge carriers between the Co3d−O2p conduction band and localized iron states is described by the equation

$$Fe_{Fe}^{\bullet} + e' \leftrightarrow Fe_{Fe}^x \quad (8)$$

In the present work, we assume for the $Sr_3FeNiO_{6+\delta}$ and $Sr_3FeCoO_{6+\delta}$ Ruddlesden−Popper phases the same model proposed by Lankhorst et al. for the $La_{0.6}Sr_{0.4}Co_{1-y}Fe_yO_{3-\delta}$ perovskite.[17] Hence, the conduction bands for $Sr_3FeNiO_{6+\delta}$ and Sr_3FeCoO_6 corresponds to those of Ni3d−O2p and Co3d−O2p, respectively.

To discuss the defect model for $Sr_3FeMO_{6+\delta}$, we will use the same reference compound as that for $Sr_3Fe_2O_{6+\delta}$,[26] $SrLa_2Fe_2O_7$. Thus, in the present work, the reference compound for oxygen excess or deficiency using the Kröger−Vink notation is expressed by $(Sr'_{La})_2(Sr_{Sr}^x)(Fe_{Fe}^x)(M_{Fe}^x)(O_O^x)_6(V_O^{\bullet\bullet})$, where (Sr'_{La}) denotes a Sr in the La site and M_{Fe}^x is a M+3 (M = Ni, Co) ion in the Fe lattice site.

The equilibrium reactions 7 and 8 lead to the following equations for the chemical potentials

$$\mu_{O_2} + 2(\mu_{V_O^{\bullet\bullet}} - \mu_{O_{O^x}}) + 4(1 - f_e)(\mu_{Fe_{Fe^x}} - \mu_{Fe_{Fe}^{\bullet}}) + 4f_e\mu_{e'} = 0 \quad (9)$$

$$\mu_{Fe_{Fe}^{\bullet}} + \mu_{e'} = \mu_{Fe_{Fe^x}} \quad (10)$$

If we assume the presence of point defects without interactions randomly distributed in the iron and oxygen lattice sites, we can define

$$\mu_{Fe} = \mu_{Fe_{Fe^x}} - \mu_{Fe_{Fe}^{\bullet}} = \mu_{Fe}^0(T) + RT\ln\left(\frac{[Fe_{Fe}^x]}{[Fe_{Fe}^{\bullet}]}\right) \quad (11)$$

$$\mu_V = \mu_{V_O^{\bullet\bullet}} - \mu_{O_{O^x}} = \mu_V^0(T) + RT\ln\left(\frac{[V_O^{\bullet\bullet}]}{[O_O^x]}\right) \quad (12)$$

The chemical potential for the charge carrier in the conduction band can be expressed through the rigid band model (RBM) formalism:[17−19]

$$\mu_{e'} = \mu_{e'}^0(T) + \frac{[e'] - [e']^0}{g(E_F)[M]} \quad (13)$$

where $\mu_{e'}^0(T)$ denotes the chemical potential of electrons when $\delta = 1$ and $[Sr'_{La}] = 0$, i.e., the chemical potential of electrons in stoichiometric $SrLa_2M_2O_7$, [e′], is the electron occupancy, $[e']^0$ is the electron occupancy for this standard condition and corresponds to an average valence 3+ for the transition metal M (M = Co, Ni), $g(E_F)$ is the density of

states at the Fermi level for the standard compound and [M] is the concentration of the transition metal; in our case, [M] = 1.

This is a straightforward approach for expressing $\mu_{e'}(T)$ as function of the electron occupancy. In this model, the M3d−O2p conduction band does not change (rigid band) with the doping level $[Sr'_{La}]$ and the oxygen vacancy concentration $[V_O^{\bullet\bullet}]$. The RBM neglects electron screening, electron correlations, exchange, and the entropy of electrons. The band is considered to be very broad, and therefore electron localization does not take place with a null contribution of electrons to the configurational entropy.

The substitution of eqs 11−13 in eq 9, which is related to eq 2, results in the following relationships

$$h_{O_2} = -2h_V^0 - 4f_e\left(h_e^0 + \frac{[e'] - [e']^0}{g(E_F)}\right) - 4(1-f_e)h_{Fe}^0 = h_{ox} - 4f_e\left(\frac{n}{g(E_F)}\right) - 4(1-f_e)\Delta h_i^0 \quad (14)$$

$$s_{O_2} = -2s_V^0 - 2R\ln\frac{[O_O^x]}{[V_O^{\bullet\bullet}]} - 4f_e s_e^0 - 4(1-f_e)\left(s_{Fe}^0 - R\ln\frac{[Fe_{Fe}^x]}{[Fe_{Fe}^{\bullet}]}\right) = s_{ox} - 2R\ln\frac{4+\delta}{1-\delta} - 4(1-f_e)\left(\Delta s_i^0 - R\ln\frac{[Fe_{Fe}^x]}{[Fe_{Fe}^{\bullet}]}\right) \quad (15)$$

where $h_{ox} = -2h_V^0 - 4h_{e'}^0$, $\Delta h_i^0 = h_{Fe}^0 - h_{e'}^0$, $s_{ox} = -2s_V^0 - 4s_{e'}^0$, and $\Delta s_i^0 = s_{Fe}^0 - s_{e'}^0$ are constants to be determined from the fitting of the h_{O_2} and s_{O_2} experimental data. s_{Fe}^0 represents the difference in entropy between the $3d^5$ (Fe3+) and $3d^4$ (Fe4+) states due to differences in degeneracy ν of both magnetic states, which gives a value of $s_{Fe}^0 = -4.25$ J mol^{-1} K^{-1}.[17]

The crystal structure of the $n = 2$ Ruddlesden−Popper phase has three different oxygen crystallographic sites labeled O(1), O(2), and O(3). O(2) corresponds to the rock-salt layer, and O(1) and O(3) are the apical and equatorial positions of the MO_6 octahedral, respectively. Neutron powder diffraction (NPD) measurements at room temperature on samples of $Sr_3Fe_2O_{6+\delta}$[9] and $Sr_3FeCoO_{6+\delta}$[10] with controlled oxygen content in the range $0 \le \delta \le 1$ indicate that the oxygen vacancies are mainly located on the O(1) crystallographic site. The situation varies when it is possible to remove oxygen atoms from the crystalline structure beyond 6.0, as happens for the $Sr_3Co_2O_{6+\delta}$[32] and $Sr_3FeCoO_{6+\delta}$[10] compounds. In this case, the analysis of the NPD measurements indicated that for $6+\delta < 6.00$, the oxygen vacancies start to be located in the O(3) crystallographic site in the equatorial plane of the octahedra as well. The oxygen crystallographic site balance for the $Sr_3FeCoO_{6+\delta}$ and $Sr_3FeNiO_{6+\delta}$ compounds depends on the different assumptions of the available oxygen crystallographic sites. This balance is 7 for O(1), O(2), and O(3), 5 for O(1) and O(3), and 1 for only O(1) oxygen lattice site.[26]

$$[V_O^{\bullet\bullet}] + [O_O^x] = 7 \text{ or } 5 \text{ or } 1 \quad (16)$$

and the iron site balance is given by

$$[Fe_{Fe}^{\bullet}] + [Fe_{Fe}^x] = 1 \quad (17)$$

The electroneutrality condition is

$$2[V_O^{\bullet\bullet}] + [Fe_{Fe}^{\bullet}] = n + [Sr'_{La}] \quad (18)$$

where $n = [e'] - [e']^0$.

The equilibrium reaction in eq 8 must still be valid after creation or removal of electrons, according to the defect reaction 7. In equilibrium, the chemical potential of electrons in both the conduction band and the electronic localized states of Fe must be in agreement with eq 10, and the variation of the chemical potential of electrons ($\mu_{e'}$ and μ_{Fe}) with their concentration must satisfy the following expression

$$f_e\frac{\partial\mu_{e'}}{\partial[e']} = -(1-f_e)\frac{\partial\mu_{Fe}}{\partial[Fe_{Fe}^{\bullet}]} \quad (19)$$

By differentiating eqs 11 and 13 and substituting into eq 19, we obtain a relationship between f_e and $[Fe_{Fe}^{\bullet}]$ is obtained

$$f_e = \left(1 + \frac{[Fe_{Fe}^{\bullet}](1-[Fe_{Fe}^{\bullet}])}{g(E_F)RT}\right)^{-1} \quad (20)$$

The electroneutrality condition in eqs 18 and 20 gives a relation between f_e, $[Fe_{Fe}^{\bullet}]$, and n. These three magnitudes depend on the oxygen content $6+\delta$. To establish a relationship of each magnitude with $6+\delta$, we assume that f_e is a function $f_e = F(6+\delta)$ that can be approached with a Taylor polynomial

$$f_e = F(6+\delta)|_6 + F'(6+\delta)|_6(\delta) + \frac{1}{2}F''(6+\delta)|_6\delta^2 + \ldots \quad (21)$$

By examination of s_{O_2} and h_{O_2} data in Figures 3 and 4, we can see that the partial molar properties are dominated by localized charge carrier at $6+\delta > 6$ and by delocalized charge carrier at $6+\delta < 6$. Therefore, the boundary conditions for f_e are

$$\lim_{\delta\to 1} f_e(6+\delta) = 0 \quad (22)$$

$$\lim_{\delta\to -\frac{1}{2}} f_e(6+\delta) = 1 \quad (23)$$

From the relation of f_e with $6+\delta$, we obtained the $[Fe_{Fe}^{\bullet}]$ and n by replacing f_e in eqs 18 and 20. The dependence of n, $[Fe_{Fe}^{\bullet}]$, $[Fe_{Fe}^x]$, and f_e as a function of $6+\delta$ is shown in Figure 5.

The fitting of h_{O_2} and s_{O_2} experimental data with eqs 14 and 15, considering the f_e, $[Fe_{Fe}^{\bullet}]$, and n relationships discussed before, leads to the determination of the parameters s_{ox}, h_{ox}, Δs_i^0, Δh_i^0, and $g(E_F)$, shown in Table 1. The fitting results are plotted in Figures 3 and 4. For comparison, in

(32) Viciu, L.; Zandbergen, H.; Xu, Q.; Huang, Q.; Lee, M.; Cava, R. *J. Solid State Chem.* **2006**, *179*, 501.

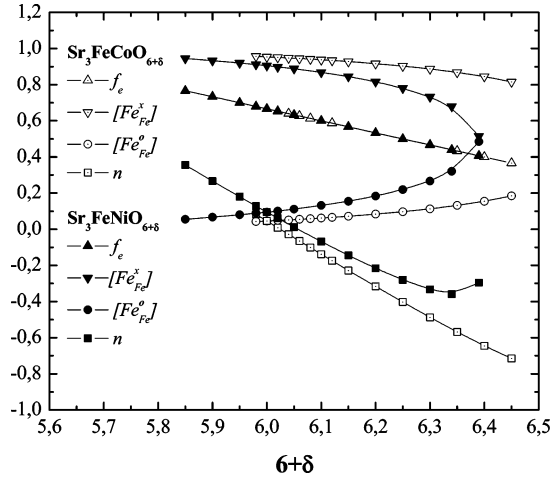

Figure 5. Dependence of n, $[Fe^{\bullet}_{Fe}]$, $[Fe^{x}_{Fe}]$, and f_e as a function of $6+\delta$, obtained from fitting of h_{O_2} and s_{O_2} data with the defect model proposed for $Sr_3FeCoO_{6+\delta}$ and $Sr_3FeNiO_{6+\delta}$ compounds.

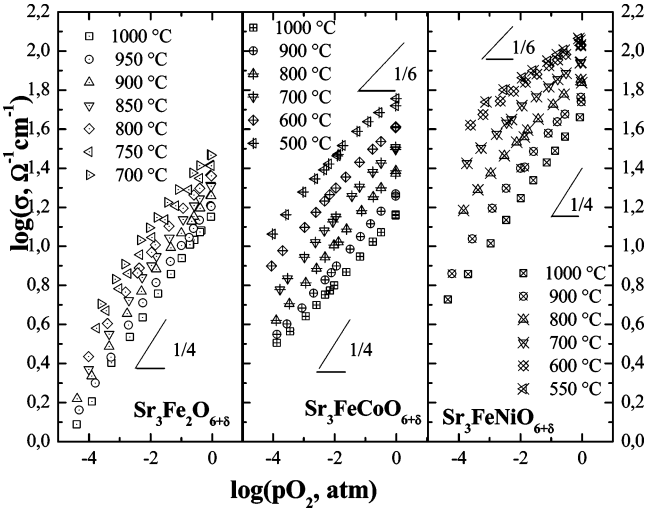

Figure 6. Isotherms of the electrical conductivity as a function of log pO_2 for $Sr_3Fe_2O_{6+\delta}$, $Sr_3FeCoO_{6+\delta}$, and $Sr_3FeNiO_{6+\delta}$ compounds.

the same table, we show the parameters s_V^0 and $h_V^0 + 2h_{Fe}^0$ obtained in ref 26 for $Sr_3Fe_2O_{6+\delta}$ and the s_{ox}, h_{ox}, Δs_i^0, Δh_i^0, and $g(E_F)$ value obtained by Lankhorst et al. for the $La_{0.6}Sr_{0.4}CoO_{3-\delta}$ and $La_{0.6}Sr_{0.4}Co_{0.4}Fe_{0.6}O_{3-\delta}$ compounds.[17−19]

The fitting values s_{ox}, h_{ox}, Δs_i^0, Δh_i^0, and $g(E_F)$, displayed in Table 1 for both $Sr_3FeNiO_{6+\delta}$ and $Sr_3FeCoO_{6+\delta}$, are close to those obtained by Lankhort et al. for $La_{0.6}Sr_{0.4}CoO_{3-\delta}$ and $La_{0.6}Sr_{0.4}Co_{0.4}Fe_{0.6}O_{3-\delta}$.[17] These values must be taken as only a rough estimation, because of the approximations used in the model to describe a complex oxide system.

3.3. Electrical Conductivity. The isotherms of electrical conductivity as a function of $\log(pO_2)$ for $Sr_3FeCoO_{6+\delta}$ and $Sr_3FeNiO_{6+\delta}$, within the range 500 °C ≤ T ≤ 1000 °C and $-5 \le \log(pO_2) \le 0$ are shown in Figure 6. The data for $Sr_3Fe_2O_{6+\delta}$ are included for comparison.

The three compounds present a positive slope for the $\log(\sigma)$ vs $\log(pO_2)$ curves. This fact suggests that the nature of charge carriers is p type. In the case of $Sr_3Fe_2O_{6+\delta}$, we attributed the transport properties to the presence of electron holes localized in the iron sites, $[Fe^{\bullet}_{Fe}]$.[26] We found a slope close to 1/4 for the limit of high temperatures and low pO_2. In this limit, $\sigma \propto [Fe^{\bullet}_{Fe}] \propto pO_2^{1/4}$, because the concentration of the other defect species is approximately constant.

The electrical behavior for $Sr_3FeCoO_{6+\delta}$ and $Sr_3FeNiO_{6+\delta}$ materials is more complex than that of $Sr_3Fe_2O_{6+\delta}$ because of the simultaneous presence of localized and itinerant charge carriers and the relation between them as we discussed above. The presence of delocalized charge carriers in the $Sr_3FeCoO_{6+\delta}$ and $Sr_3FeNiO_{6+\delta}$ materials should be responsible for the diminuation of the $\log(\sigma)$ vs $\log(pO_2)$ slope with respect to those observed for $Sr_3Fe_2O_{6+\delta}$ at the high pO_2 and low T limit (see Figure 6).

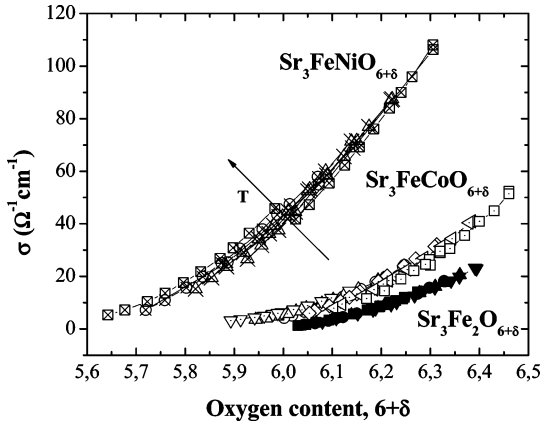

Figure 7. Electrical conductivity σ as a function of $6+\delta$ for $Sr_3Fe_2O_{6+\delta}$, $Sr_3FeCoO_{6+\delta}$, and $Sr_3FeNiO_{6+\delta}$ compounds at several temperatures.

By combination of electrical conductivity and thermogravimetric data, we can establish an experimental relation between σ and the oxygen nonstoichiometry $6+\delta$ for $Sr_3Fe_2O_{6+\delta}$, $Sr_3FeCoO_{6+\delta}$, and $Sr_3FeNiO_{6+\delta}$. This relation at different temperatures is shown in Figure 7. It can be seen that for a given oxygen content value, the electrical conductivity for the three compounds increases as T increases, showing a thermally activated behavior. The electrical conductivity increases according to the series Fe < Co < Ni.

In the $Sr_3Fe_2O_{6+\delta}$ compound, we propose that the electrical conductivity is associated with the presence of small polarons ($[Fe^{\bullet}_{Fe}]$) with a mobility term given by[26]

$$\mu_p^{SP} = \frac{A}{T^{3/2}} \exp\left(-\frac{E_a}{kT}\right) \qquad (24)$$

We found that for $[Fe^{\bullet}_{Fe}] < 0.28$, $\mu_p^{SP} \approx 0.015$ cm^2 V^{-1} s^{-1} with $E_a \approx 0.2$ eV and $A \approx 4174$ cm^2 K$^{3/2}$ V^{-1} s^{-1}.

Table 1. Fitting Values, s_{ox}, h_{ox}, Δs_i^0, Δh_i^0 and $g(E_F)$ for $Sr_3FeNiO_{6+\delta}$, $Sr_3FeCoO_{6+\delta}$ (our data), $Sr_3Fe_2O_{6+\delta}$ (Mogni et al.[26]), $La_{0.6}Sr_{0.4}CoO_{3-\delta}$, and $La_{0.6}Sr_{0.4}Co_{0.4}Fe_{0.6}O_{3-\delta}$ (Lankhort et al.[17])

	h_{ox} (kJ/mol)	Δh_i^0 (kJ/mol)	s_{ox} J/mol K)	Δs_i^0 (J mol^{-1} K^{-1})	$g(E_F$ ((kJ/mol)$^{-1}$)	s_V^0 (J mol^{-1} K^{-1})	$h_V^0 + 2h_{Fe}^0$ (kJ/mol)
$Sr_3Fe_2O_{6+\delta}$						−51	74
$Sr_3FeNiO_{6+\delta}$	−189 ± 12	−11 ± 7	70 ± 3	−4.25	0.0206	−35	73
$Sr_3FeCoO_{6+\delta}$	−188 ± 37	11 ± 29	77 ± 5	−4.25	0.0105	−39	116
$La_{0.6}Sr_{0.4}CoO_{3-\delta}$	−281	−25	86	−4.25	0.0153	−43	91
$La_{0.6}Sr_{0.4}Co_{0.4}Fe_{0.6}O_{3-\delta}$	−314	−25	83	−4.25	0.0153	−41	107

Assuming localized electronic states in the Fe sites for $Sr_3FeCoO_{6+\delta}$ and $Sr_3FeNiO_{6+\delta}$ and small polarons (SP) associated with this site, we can calculate its contribution to the total electrical conductivity by

$$\sigma^{SP} = x_p^{SP} e\left(\frac{A_v}{V_{u.c.}}\right)\mu_p^{SP} \quad (25)$$

where e is the electron charge, A_v is Avogadro's number, $V_{u.c.}$ is the unit cell volume, and $x_p^{SP} = [Fe_{Fe}^{\bullet}]$ is the small polaron concentration shown in Figure 5. From eq 25, we can estimate a maximum contribution of the small polaron conductivity to the total conductivity of around 1 and 3 $\Omega^{-1}cm^{-1}$ for the $Sr_3FeCoO_{6+\delta}$ and $Sr_3FeNiO_{6+\delta}$ compounds, respectively. This fact suggests that we can neglect the contribution of small polaron conductivity due to Fe states to the total conductivity σ.

In section 3.2, we discussed a defect model for $Sr_3FeCoO_{6+\delta}$ and $Sr_3FeNiO_{6+\delta}$ compounds using the f_e fraction of the delocalized charge carrier in the Co3d−O2p or Ni3d−O2p band, respectively. Keeping this fact in mind along with the observed higher values of electrical conductivity respect to that of $Sr_3Fe_2O_{6+\delta}$, we analyze the contribution of delocalized charge carriers as large polaron (LP) type.

In the LP type conductivity, the charge-carrier/phonon interaction is weaker than that of SP and the charge carriers move in a conduction band with a higher effective mass because of the drag of their polarization cloud. The electrical conductivity thus presents a thermally activated behavior mainly due to the LP energy formation E_f. In this frame, the charge carriers are not localized in the crystal lattice, and consequently, they do not contribute to the configurational entropy as it was deduced from the partial molar properties.

The electrical conductivity for electron holes in the frame of the large polarons (LP) theory is given by

$$\sigma^{LP} = x_p^{LP} e\left(\frac{A_v}{V_{u.c.}}\right)\mu_p^{LP} = (x_p^{LP})^0 e\left(\frac{A_v}{V_{u.c.}}\right)\mu_p^{LP} \exp\left(-\frac{E_f}{kT}\right) \quad (26)$$

where x_p^{LP} is the electron hole charge-carrier concentration contributing to the electrical conductivity as large polarons, E_f is the LP energy formation, and μ_p^{LP} is the large polaron mobility in the M3d−O2p conduction band given by

$$\mu_p^{LP} = \frac{B}{T^{1/2}} \quad (27)$$

where B is a general constant.

The E_f vs $6+\delta$ data for the $Sr_3FeCoO_{6+\delta}$ and $Sr_3FeNiO_{6+\delta}$ compounds obtained from the slopes of $\ln(\sigma T^{1/2})$ vs $1/T$ data (not shown here) are displayed in Figure 8. The E_f values obtained for the $Sr_3FeNiO_{6+\delta}$ compound are lower than those of $Sr_3FeCoO_{6+\delta}$, which is in agreement with their higher electrical conductivity. A rapid increase in E_f can be observed as $6+\delta$ decreases from 6.00. This behavior can be associated with a significant contribution for $6+\delta < 6.00$ of the oxygen vacancies in the O(3) equatorial crystal site[26] in addition to the expected oxygen vacancies in the O(1) site.[9,10,32]

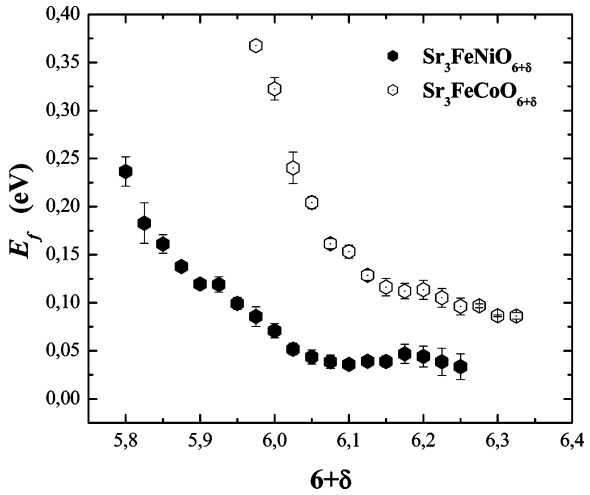

Figure 8. Energy of LP formation, E_f, as a function of $6+\delta$ for $Sr_3FeCoO_{6+\delta}$ and $Sr_3FeNiO_{6+\delta}$ compounds.

A value for the charge carrier mobility for the LP model can be roughly estimated from eq 26, using σ, the oxygen content, the activation energy, and the unit-cell volume determined by XRD. Assuming for the $n = 2$ Ruddlesden−Popper compound the same electronic configuration as that of perovskites at high temperatures,[33] we can express the Ni3+ and Co3+ electronic states as $t_2^6e^1 \rightarrow t_2^6\sigma^{*1}$ and $t_2^5e^1 \rightarrow t_2^5\sigma^{*1}$, respectively. σ^* denotes a hybrid Me−O2p orbital for the mixed-valence case where the number of electrons is given by $1 + n$ (see 3.2) and the number of holes (x_p^0) for this conduction band by $2 - (1 + n)$. In our case, the values of n as a function of the oxygen content are estimated from the defect model shown in Figure 5.

From the energy of LP formations and the conductivity data plotted in Figures 7 and 8, we obtain compound mobility values of $0.46 \geq \mu_p^{LP} \geq 0.10$ cm^2 V^{-1} seg^{-1} within the interval $6.00 < 6+\delta < 6.3$ for $Sr_3FeCoO_{6+\delta}$ and $0.31 \geq \mu_p^{LP} \geq 0.21$ cm^2 V^{-1} seg^{-1} between $5.8 < 6+\delta < 6.2$ for $Sr_3FeCoO_{6+\delta}$. On the other hand, if we assume that the charge carriers are small polaron and revaluate E_f with this assumption from the slope of the $\log(\sigma T^{3/2})$ vs $1/T$ curves (not shown here), the mobility values for $Sr_3FeCoO_{6+\delta}$ compound are in the range $1.12 \geq \mu_p^{SP} \geq 0.27$ cm^2 V^{-1} seg^{-1} within the interval $6.00 < 6+\delta < 6.3$ and for $Sr_3FeNiO_{6+\delta}$ $1.82 \geq \mu_p^{SP} \geq 0.68$ cm^2 V^{-1} seg^{-1} between $5.8 < 6+\delta < 6.2$. The mobility values for large polarons are generally on the order of 1−10 cm^2 V^{-1} s^{-1}, whereas those for small polaron mobilities are between 1×10^{-4} and 1×10^{-1} cm^2 V^{-1} s^{-1}. The estimated mobilities for both $Sr_3FeCoO_{6+\delta}$ and $Sr_3FeNiO_{6+\delta}$ compounds in either the frame of large polaron or small polaron behavior are between these values. Consequently, it is difficult to infer the exact nature of the charge carriers solely from this estimation. However, the high-temperature thermodynamic data, s_{O_2} and h_{O_2}, also provide information on the nature of the charge carriers, as we discussed above. The charge-carrier delocalization suggested by the dependence of s_{O_2} and h_{O_2} on the $6+\delta$ data gives an additional insight for a charge-carrier conduction mechanism of the large polaron type.

(33) Goodenough, J. B. *Rep. Prog. Phys.* **2004**, *67*, 1915.

4. Conclusions

For the $Sr_3Fe_2O_{6+\delta}$ compound, the thermodynamic properties suggest a stabilization of the $Sr_3Fe_2O_6$ composition with all Fe as Fe+3. The partial substitution of Fe by Co or Ni prevents this stabilization by increasing the oxygen nonstoichiometry range. The oxygen-vacancy range is improved with the $Sr_3Fe_2O_{6+\delta} < Sr_3FeCoO_{6+\delta} < Sr_3FeNiO_{6+\delta}$ series.

For the starting material $Sr_3Fe_2O_{6+\delta}$, the description of the defect structure is easier than that of $Sr_3FeMO_{6+\delta}$ (M= Co, Ni) compounds because of the existence of a unique transition-metal species with two possible oxidation states, Fe3+/Fe4+. For this reason, a straightforward defect model assuming localized charge carriers and oxygen vacancies allows for a good fitting of the experimental results. $Sr_3FeMO_{6+\delta}$ (M = Co, Ni) presents a more-complicated analysis because it has two different transition-metal species, both with two or more oxidation states. The partial molar enthalpy (h_{O_2}) and entropy (s_{O_2}) data of $Sr_3FeCoO_{6+\delta}$ and $Sr_3FeNiO_{6+\delta}$ compounds are discussed using a straightforward defect model on the basis of the mass action law assuming oxygen-vacancy formation involving different fractions of localized and delocalized charge carriers in iron sites and the transition-metal M3d−O2p band, respectively. Despite its simplicity, this model and our previous work on the $Sr_3Fe_2O_{6+\delta}$ material provide a way for the understanding of the complex defect and electronic structure of the $Sr_3FeMO_{6+\delta}$ (M = Co, Ni) compounds.

The combination of the high-temperature thermodynamic and conductivity data allows for the determination of the dependence of the electrical conductivity with the oxygen content at several temperatures. The electrical conductivity is thermally activated and, at fixed oxygen content, increases with the $Sr_3Fe_2O_{6+\delta} < Sr_3FeCoO_{6+\delta} < Sr_3FeNiO_{6+\delta}$ series. This is in agreement with the enhanced covalency of M−O bonding from the left to the right in a transition metal series. The estimated mobilities for $Sr_3FeCoO_{6+\delta}$ and $Sr_3FeNiO_{6+\delta}$ compounds are between the typical values for large polaron and small polaron type behavior. The charge-carrier delocalization suggested by the dependence of s_{O_2} and h_{O_2} on $6+\delta$ data gives an additional insight for a charge-carrier conduction mechanism of the large polaron type.

Acknowledgment. The authors are indebted to Professor B. Alascio for valuable discussion. They also gratefully acknowledge the help of Dr. M. Esquivel in the English revision of this manuscript. This work was supported by CNEA (Atomic Energy National Commission), CONICET (Argentine Research Council), Antorchas Foundation (Argentina), and ANPCyT (National Agency of Promotion Science and Technology) through PICT 12-14493.

CM0604007